Pulse Laser Deposition and Electrochemical Characterization of LiFePO4−C Composite Thin Films

ARTICLE *in* THE JOURNAL OF PHYSICAL CHEMISTRY C · APRIL 2008

Impact Factor: 4.77 · DOI: 10.1021/jp0744735

3 AUTHORS:

Zhouguang Lu
South University of Science and Technology …
83 PUBLICATIONS **1,444** CITATIONS
SEE PROFILE

Ming-Fai Lo
City University of Hong Kong
50 PUBLICATIONS **779** CITATIONS
SEE PROFILE

Jonathan C.Y. Chung
City University of Hong Kong
200 PUBLICATIONS **2,717** CITATIONS
SEE PROFILE

Pulse Laser Deposition and Electrochemical Characterization of $LiFePO_4$−C Composite Thin Films

Z. G. Lu, M. F. Lo, and C. Y. Chung*

Department of Physics and Materials Science, City University of Hong Kong, Tat Chee Avenue, Kowloon, Hong Kong SAR, People's Republic of China

Received: June 9, 2007; In Final Form: January 15, 2008

Conductive carbon was codeposited with $LiFePO_4$ to enhance the electrical conductivity of the olivine-type $LiFePO_4$ thin films. In this approach, poly(vinyl alcohol) was used as the source for carbon as well as the binder for target densification. After a highly densified (>80%) $LiFePO_4$−C target was fabricated, pulse laser deposition (PLD) technique was employed to deposit the $LiFePO_4$−C composite thin films on the Si/SiO_2/Ti/Pt substrates. The as-deposited $LiFePO_4$−C composite films were characterized by techniques of X-ray diffraction, scanning electron microscopy, Raman scattering spectroscopy, X-ray photoelectron spectroscopy, DC conductivity measurement, as well as cyclic voltammograms, electrochemical impedance spectroscopy, and galvanostatics. The effects of carbon content and postdeposition annealing treatments on the electrochemical performances of the as-deposited film electrodes were carefully investigated. The results showed that the codeposited carbon was homogeneously distributed throughout the $LiFePO_4$ films. It was found that 2 mol% carbon was the optimized amount for the highest capacity. Postdeposition annealing at 600 °C for 6 h in the same vacuum chamber could considerably improve the Coulombic efficiency as well as the high rate capability of the PLD-deposited $LiFePO_4$−C composite thin films. However, the specific capacity would be reduced.

1. Introduction

Since Padhi et al.[1] reported the promising use of olivine-type $LiFePO_4$ as a cathode for Li ion batteries in 1997, this class of compounds known as phospho-olivines has attracted tremendous attention. The main advantages of $LiFePO_4$ include the flat voltage plateau (∼3.4 V versus Li^+/Li), moderate theoretical specific capacity (170 mAh/g), thermal stability, long cycling life, and most importantly, environmental friendliness and abundance of Fe resources in nature. From a safety point of view, the superiority of $LiFePO_4$ over other cathode materials such as $LiCoO_2$, $LiNiO_2$, and $LiMn_2O_4$ lies in its outstanding tolerance against overcharging and overdischarging.[1−3]

However, $LiFePO_4$ strongly suffers from its limited high rate capability because of its intrinsic low electrical conductivity (∼10^{-9} to 10^{-10} S·cm^{-1}) and low Li^+ ion diffusion.[1−3] In the past decade, tremendous efforts had been devoted to tackle these problems. Two primary important approaches for enhancing the real electrical conductivity include coating the $LiFePO_4$ particles with a thin layer of conductive carbon[4,5] and substituting lithium with supervalent metals.[6] On the other hand, fabricating ultrafine $LiFePO_4$ nanoparticles with uniform particle shape and size distribution via wet-chemical routes was also proved a feasible method to enhance the Li^+ diffusion.[7−9]

Thin film electrodes are of great interest because they can serve as a simplified model for elaborating the detail electrochemical process of their counterpart active materials.[10] Thin film electrodes with thickness ranging from a few to hundreds of nanometers are also essential for solid-state microbatteries, especially in low power applications, as the active or standby power sources for microelectronics such as nonvolatile memory, semiconductor diagnostic wafers, smart cards, remote sensors, radio frequency identification tags, miniature transmitters, and biomedical implantable defibrillators, drug delivery systems, and neural stimulators.[11−14] As compared with the conventional film cathode of $LiCoO_2$, the olivine $LiFePO_4$ film cathode is unique because it is totally environmentally friendly and nontoxic. This is particularly important when it is used as the energy storage for medical devices.

There are several reports on the growth of olivine $LiFePO_4$ thin films via pulse laser deposition (PLD),[10,15−19] radio frequency (RF) magnetron sputtering,[20,21] or electrostatic spray deposition (ESD) combined with sol−gel methods.[22] It was speculated that low electrical conductivity was no longer a critical problem in the case of an electrode with thickness of a few hundred nanometers since the electron and ion can be instantly transported and diffused through the very thin electrode layer into the Pt current collectors and the electrolytes.[15,16] However, previous results showed that the as-deposited pristine $LiFePO_4$ thin films without any postdeposition treatments (annealing or surface scratching) presented very limited discharge capacity and poor high rate capability.[10,15−25] On the other hand, the codeposition of conductive carbon,[20] silver,[23] or gold[24] obviously improved the electrochemical performances, because the presence of carbon or gold can enhance the electrical conductivity of the $LiFePO_4$ films. The main objective of this article is to study the effects of various amounts of codeposited carbon and the subsequent postdeposition annealing treatments on the electrochemical performances of the $LiFePO_4$ thin films.

2. Experimental Procedures

2.1. PLD Target Preparation. *2.1.1. $LiFePO_4$ Raw Materials Preparation.* A simple hydrothermal process similar to that in

* To whom correspondence should be addressed. Tel.: 852-27887835. Fax: 852-27887830. E-mail: appchung@cityu.edu.hk.

10.1021/jp0744735 CCC: $40.75
Published on Web 04/10/2008

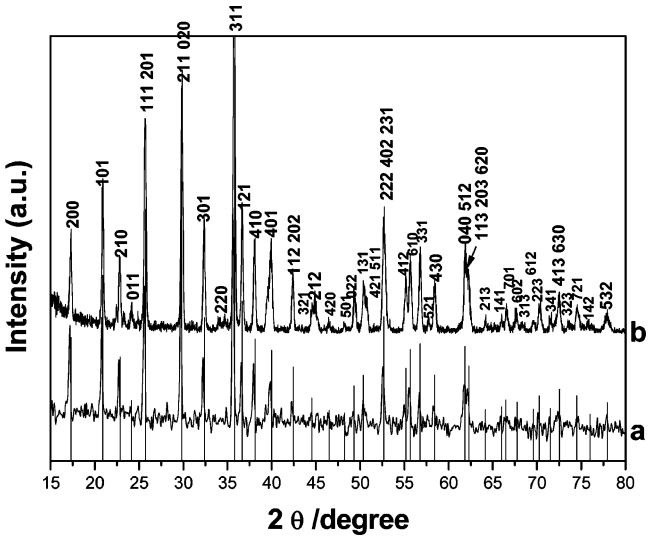

Figure 1. XRD patterns of the $LiFePO_4$ (a) raw materials and (b) the as-sintered $LiFePO_4$−C target. The lines below are the position of the diffraction peaks of the standard olive-type $LiFePO_4$ according to JCPDS-832092.

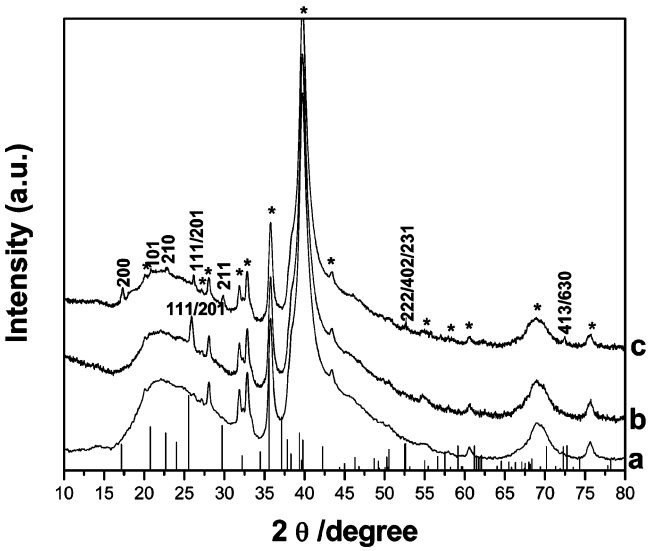

Figure 2. XRD patterns of the (a) $Si/SiO_2/Ti/Pt$ substrate and the as-deposited $LiFePO_4$−C thin film (b) before and (c) after postdeposition annealing at 600 °C for 6 h. The lines below are the position of the diffraction peaks of the standard olive-type $LiFePO_4$ according to JCPDS-832092.

ref 26 was employed to prepare the olivine-type $LiFePO_4$ ultrafine particles serving as raw materials. The starting chemicals were lithium hydroxide monohydrate ($LiOH{\cdot}H_2O$), ammonium ferrous sulfate [$Fe(NH_4)_2(SO_4)_2{\cdot}6H_2O$], ammonium dihydrogen phosphate ($NH_4{\cdot}H_2PO_4$), and poly(vinylpyrrolidone) (PVP) (C_6H_9NO). All chemicals were used as received without further purification. The stoichiometric ratio of Li/Fe/P in the precursor solution was fixed to 3:1:1.

In a typical procedure, PVP, $LiOH{\cdot}H_2O$, $Fe(NH_4)_2(SO_4)_2{\cdot}6H_2O$, and $NH_4{\cdot}H_2PO_4$ were dissolved in 10 mL of distilled water at room temperature separately. They were stirred for approximately 30 min to ensure complete dissolution. PVP and $Fe(NH_4)_2(SO_4)_2{\cdot}6H_2O$ solutions were mixed together. The $NH_4{\cdot}H_2PO_4$ solution was then added to the resulting solution under constant stirring. The solution was then left for reaction for at least 30 min. After that, the $LiOH{\cdot}H_2O$ solution was added slowly under vigorous stirring to produce a light green slurry. After being mixed homogeneously, the pH value of the slurry

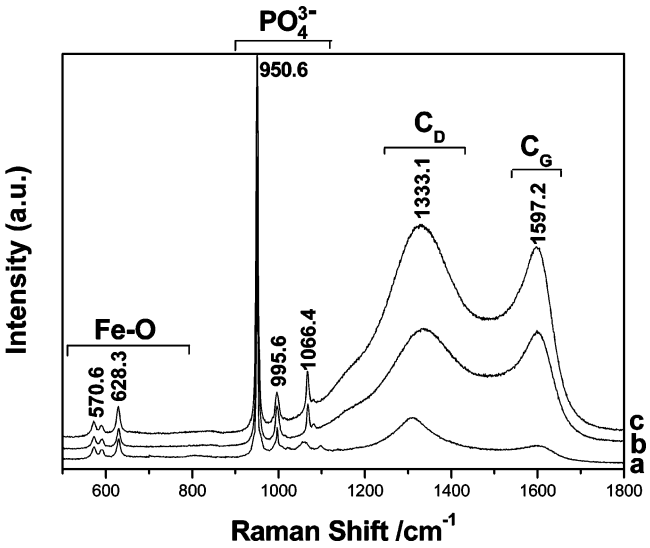

Figure 3. Raman spectra of the as-sintered $LiFePO_4$−C (a) target A, (b) target B, and (c) target C with 0.5, 2.0, and 3.0 wt % PVA, respectively.

was approximately neutral. The slurry was then stirred for 5 min and quickly transferred into an autoclave, which was sealed and heated at 150 °C for 6 h. During this hydrothermal process, $LiFePO_4$ crystallization took place inside the sealed autoclave. Subsequently, the autoclave was naturally cooled to room temperature and the resulting gray precipitates were filtered and dried at 80 °C for 12 h to yield the $LiFePO_4$ raw powder materials.

2.1.2. $LiFePO_4$−C Target Preparation. In this study, an investigation about the influences of the amount of conductive carbon on the thin film cathode electrochemical properties was conducted. Poly(vinyl alcohol) (PVA) was used as the source of carbon as well as binder for the target densification. The percentage of carbon included in the target was controlled by the amount of PVA used. Three different amounts, 0.5, 2.0, and 3.0 wt %, of PVA were homogeneously mixed with the as-synthesized $LiFePO_4$ powders (the corresponding targets were denoted as targets A, B, and C, respectively) and then dried at 80 °C for 10 h. The dried powders were ground uniformly and cold pressed into 2.5-cm pellets using a hydraulic press at a pressure of 5 MPa, which was then sintered at 800 °C for 20 h in an argon atmosphere to yield a target with a relative density of about 85%.

2.2. Pulsed Laser Deposition of $LiFePO_4$−C Composite Thin Films. A stainless steel vacuum chamber equipped with a rotating holder for both target and substrate was used to deposit the $LiFePO_4$−C thin films on $Si/SiO_2/Ti/Pt$ substrates. A laser beam of 248 nm in wavelength was provided by a KrF excimer laser source (Lambda Physik LPX 200), which was focused onto the rotating $LiFePO_4$−C target. For all the experiments described in this work, the laser energy, laser impulsion frequency, and substrate temperature were fixed at 300 mJ (~2 J cm^{-2}), 10 Hz, and 600 °C, respectively. The substrate−target distance was set at 3 cm. Before deposition, the vacuum chamber was evacuated to a backing pressure of 1×10^{-6} mbar, and then the working pressure was kept at 0.15 mbar through a pressure controller by using high purity argon (99.99%) as the protection gas. After PLD deposition for 1 h, the chamber was naturally cooled to room temperature before the vacuum was broken and the as-deposited $LiFePO_4$−C films were collected.

2.3. Heat Treatments of the $LiFePO_4$−C Composite Films. For the in-chamber postdeposition annealing treatment, after the

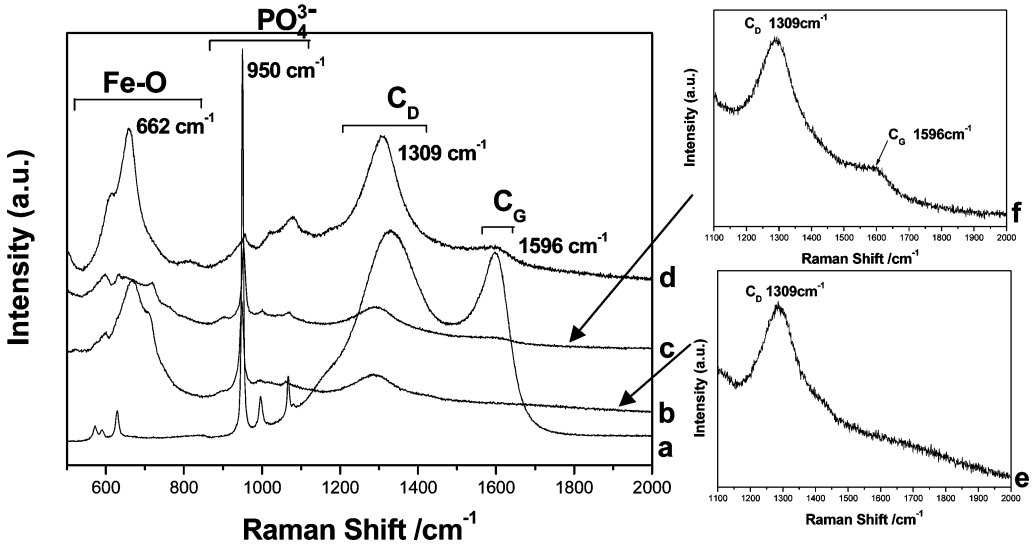

Figure 4. Raman spectra of the $LiFePO_4$−C (a) target C and (b) the thin films deposited from the target C before annealing, (c) after annealing at 600 °C for 6 h, and (d) the film without annealing after charge/discharge cycling for 115 times. (e, f) Enlarged parts from 1100 to 2000 cm^{-1} of (b) and (c), respectively.

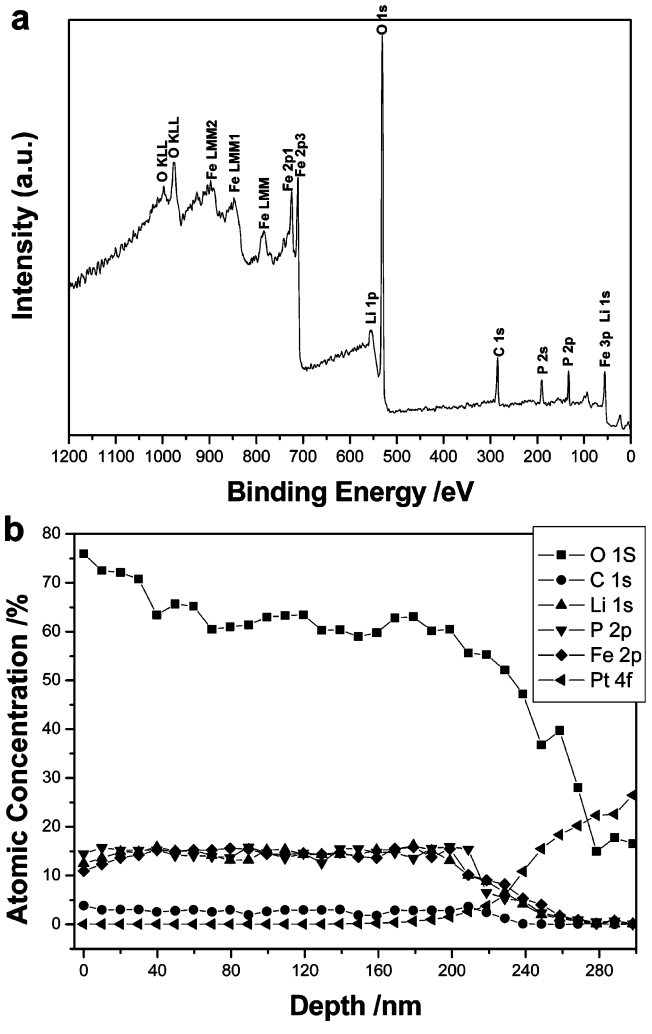

Figure 5. (a) Survey XPS of the as-deposited $LiFePO_4$−C thin films. (b) XPS depth profiling of the as-deposited $LiFePO_4$−C composite thin film with average sputtering rate of 19.88 nm/min.

laser was turned off, the as-deposited $LiFePO_4$−C composite films were kept in the chamber, which was maintained at the temperature of 600 °C for 6 h.

2.4. Characterization of the $LiFePO_4$−C Composite Thin Films. The X-ray diffraction (XRD) patterns were recorded in a $\theta/2\theta$ configuration using a Siemens D500 powder diffractometer equipped with Cu Kα radiation ($\lambda = 1.5405$ Å). The surface morphologies and the thickness of the films were characterized using a field emission scanning electron microscope (JEOL JSM-6334F). X-ray photoelectron spectroscopy (XPS, PHI model 5802) and Raman spectroscopy (Spex Rama Log 1403) were employed to verify the composition and chemical bonding characteristics of the as-deposited $LiFePO_4$−C thin films.

2.5. Electrical Conductivity and Electrochemical Characterization. The electrical conductivities were measured at room temperature (25 °C) via the two-probe DC methods on a Keithley 237 setup. For electrical contact, nine spherical gold electrodes of 2 mm in diameter and 50 nm in thickness were sputtered on top of the $LiFePO_4$−C films (Figure S1). Nine parallel experiments were conducted by varying the gold electrodes, and then the mean values were obtained to increase the measurement accuracy.

A three-electrode system was employed to characterize the electrochemical performances of the as-deposited $LiFePO_4$−C composite thin films. The electrolyte used was 1 M $LiClO_4$ dissolved in propylene carbonate. Lithium metal foil was used as the counter and reference electrodes as well. The data were collected on an automatic Versastat II EG&G system, and all the electrochemical characterizations were carried out in a glovebox under high purity argon gas protection. The freshly deposited $LiFePO_4$−C films with the same experimental parameters were used for the cyclic voltammogram (CV) testing and normal charging and discharging experiments, as well as for the high rate charge and discharge characterization. Owing to the difficulty in accurately evaluating the weight of the as-deposited $LiFePO_4$−C composite thin films on $Si/SiO_2/Ti/Pt$ substrates, here we report on specific capacities in terms of the $\mu Ah \cdot \mu m^{-1} \cdot cm^{-2}$ unit instead of the normally employed unit of $mAh \cdot g^{-1}$. All the electrochemical measurements were carried out at room temperature (25 °C). The electrochemical impedance spectra (EIS) measurements were performed over a frequency range of 0.001 Hz to 1 MHz at a 50% discharge stage, with a perturbation signal of 5 mV over a Chi 660c setup.

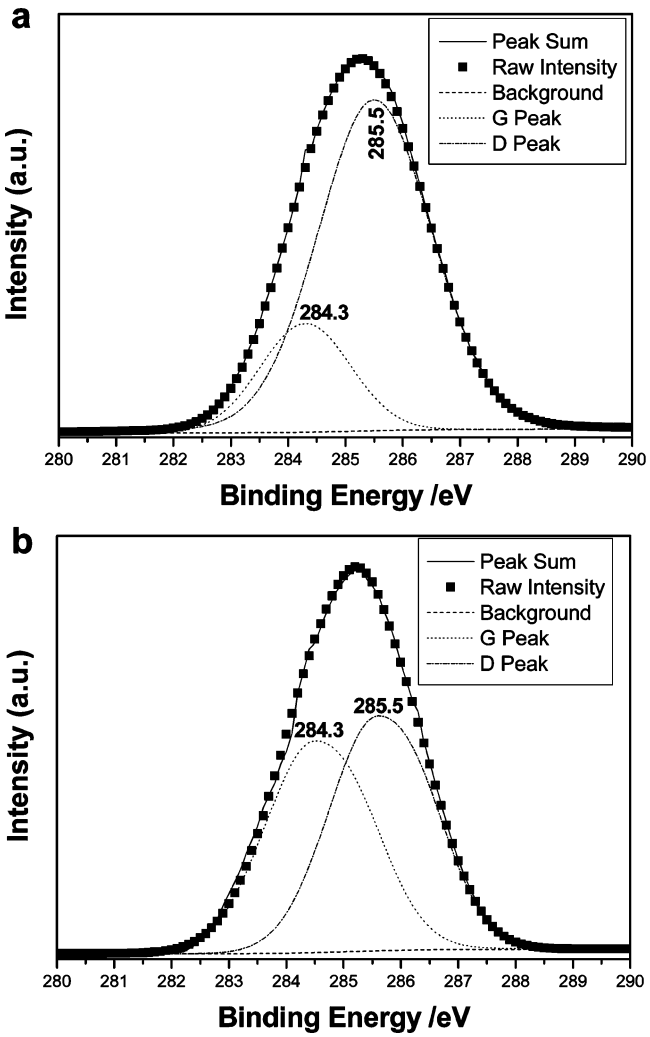

Figure 6. High resolution and deconvolved XPS for the C 1s signal of the $LiFePO_4$−C films deposited from target C (a) before and (b) after annealing treatment. The film was subjected to ion-beam sputtering for 2 min before the data were collected.

3. Results and Discussion

3.1. Physical Characterization. *3.1.1. XRD Analysis.* Figure 1 shows the XRD pattern of the hydrothermally synthesized $LiFePO_4$ raw materials and the sintered target. All the peaks can be indexed as the olivine phase $LiFePO_4$, which indicates that the materials formed were single-phase well-crystallized $LiFePO_4$. Phase purity of the as-made $LiFePO_4$−C target is confirmed in line b. As compared to the raw materials, the crystallinity of the target is much improved because of the high calcination temperature used in the target densification process. It was noted that no diffraction peaks corresponding to the carbon could be seen in the XRD patterns. This implies that the content of carbon in the $LiFePO_4$−C target might be less than 5% or that the carbon exists in an amorphous state.

Figure 2 reveals significant crystallographic changes of the as-deposited $LiFePO_4$−C composite films after annealing. For films before annealing (line b), we can observe only one diffraction peak at the angle around 25.8°, corresponding to the (111)/(201) crystal plane of the olivine $LiFePO_4$ (JCPDS-832092). This implies a preferentially oriented growth of the as-deposited films. After annealing (line c), in addition to the weakening of the (111)/(201) diffraction peak, the diffraction peaks ascribing to the planes of (200), (101), (210), (211), (101), (222)/(402)/(231), and (413)/(630) became stronger. This suggests that postdeposition heat treatment had changed the texture of the film, which might affect the electrochemical activities a lot. The phenomenon will be discussed again in the following section.

3.1.2. Raman Analysis. Figure 3 shows the variation of the Raman spectra of the as-sintered $LiFePO_4$−C targets as a function of carbon content. The peaks centered at 1333.1 and 1597.2 cm^{-1} are specific to the D band (sp^3) and G band (sp^2) of the carbon structure, respectively.[18,19] The D and G fractions were estimated by fitting the Raman spectrum. Each component is a convolution of Gaussian distribution, and the contribution of the background was subtracted by the Shirley method. The integral intensity ratios of the G band to D band of targets A, B, and C were estimated to be about 0.17, 0.93, and 0.97, respectively. It means that the G/D ratio increases with the carbon content in the as-prepared $LiFePO_4$−C targets. The sharp band at 950.6 cm^{-1} altogether with 995.6 and 1066.4 cm^{-1} can be attributed to the symmetric PO_4^{3-} stretching vibration of $LiFePO_4$.[10] The peaks distributed around 600 cm^{-1} can be attributed to iron oxide which probably had been formed on the surface resulting from the disproportionation of $LiFePO_4$ to $FePO_4$, which was also observed and reported in previous reports.[10,27,28]

Figure 4 shows the Raman spectra of the $LiFePO_4$−C composite films deposited using target C. For comparison, the Raman spectrum of target C is also included in the figure (line a). As compared with the target, the film deposited from it without annealing (line b) shows the characteristic PO_4^{3-} peak at around 950 cm^{-1}. Noticeably, only the D band signal can be observed in the carbon range (line e). Since sp^3 bonding signifies the nonconductive form of carbon, the electrical conductivity of the as-deposited $LiFePO_4$−C composite thin film is believed to be not so good, which should result in a relatively poor electrochemical high rate capability to be discussed later. However, after annealing treatment, a very weak and broad vibration due to conductive sp^2-bonded carbon appears at around 1596 cm^{-1} (lines c and f). The integral G/D ratio of the film deposited using target C was increased from less than 0.05 before annealing to 0.20 after annealing. The annealed film with higher G/D ratio of carbon should have better electrical conductivity. Figure 4d shows the typical Raman spectrum of the $LiFePO_4$−C composite film without annealing and after charge/discharge cycling for 115 times. It was found that the vibrations belonging to carbon (D and G bands) and iron oxide become more prevalent while the characteristic vibration due to the $LiFePO_4$ structure was weakened. It was speculated that the decomposition of the electrolytes and the disproportionation from $LiFePO_4$ to $FePO_4$ were the reasons behind these phenomena.

3.1.3. XPS Analysis. Before collecting the XPS data (except for the depth profiling), the $LiFePO_4$−C composite film was subjected to ion-beam sputtering for 2 min (about 40 nm) to remove the surface contaminations. Figure 5a shows a full-scale XPS of the $LiFePO_4$−C composite thin film deposited from target C without annealing treatment. It reveals the signatures of the carbon and $LiFePO_4$. Figure 5b shows the atomic concentrations of the Li, Fe, P, O, C, and Pt elements as a function of depth perpendicularly to the film surface. It indicates that the as-deposited $LiFePO_4$ film thickness was about 200 nm and the composition was uniform through the film thickness. The atomic concentration of carbon in the as-deposited $LiFePO_4$−C composite film was calculated to be about 2 mol%, and the molar ratio of Li/Fe/P/O was near 1:1:1:4. Most

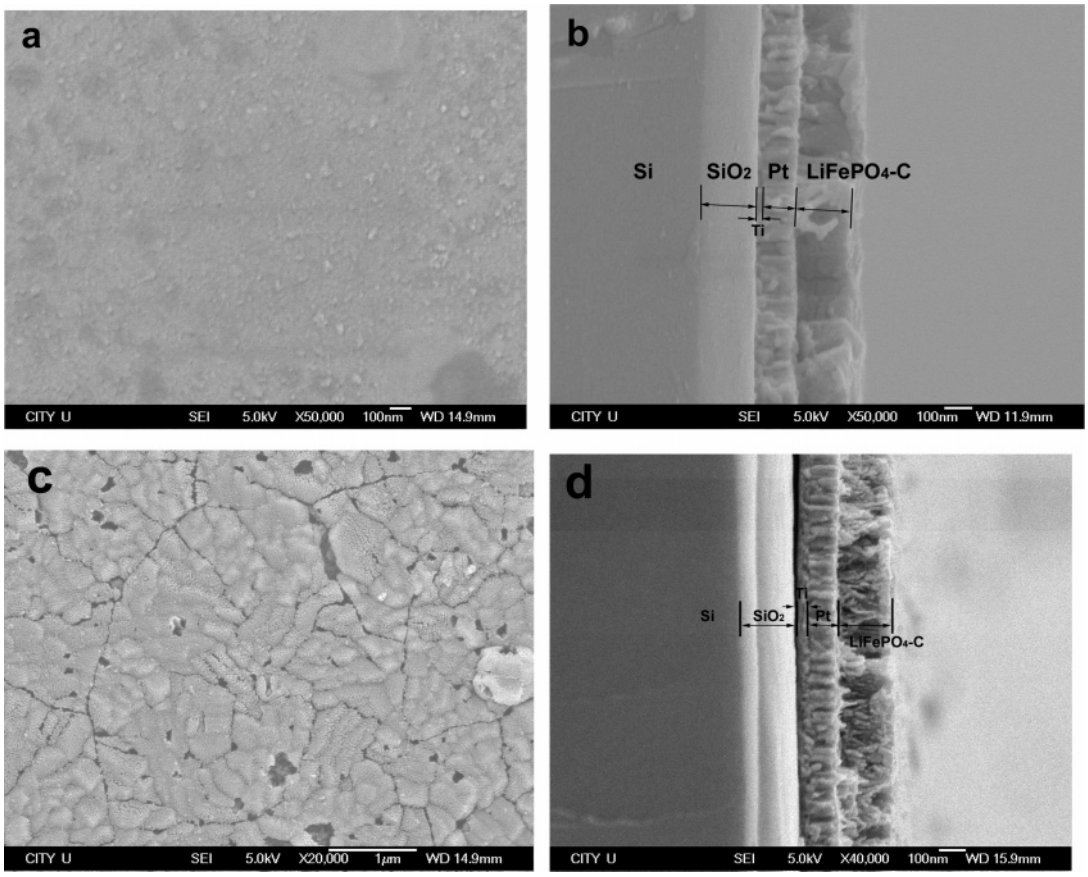

Figure 7. (a, c) Plan-view and (b, d) cross section SEM images of the $LiFePO_4$−C thin films deposited using target C. (a, b) Before and (c, d) after annealing treatment at 600 °C for 6 h.

importantly, carbon is distributed uniformly in the as-deposited $LiFePO_4$−C composite film.

Full-scale XPS analysis showed no obvious differences between the $LiFePO_4$−C films before and after the annealing treatment. To get detailed information about the sp^2/sp^3 coordination of carbon in the as-deposited $LiFePO_4$−C composite films, high-resolution XPS analysis of the C 1s signal was performed, and the results are shown in Figure 6, which indicates some noticeable differences between these two sets of samples. Figure 6 also presents the deconvolved results of the C 1s XPS signals before and after the annealing treatment. The sp^2 and sp^3 fractions were estimated from the XPS fitting curves, consisting of peaks due to the D band (285.5 eV) and G band (284.3 eV).[29] Each component is a convolution of a Gaussian and a Lorentzian method, and the contribution of the background was approximated by the Shirley method. The fractions of the G band of the film before and after annealing treatment were estimated to be about 12% and 45%, respectively. It is believed that the electrical conductivity of the $LiFePO_4$−C film can be improved with increase in the volume fraction of conductive sp^2-bonding carbon after annealing. However, as mentioned in the Raman analysis, no sp^2-coordinated carbon was observed in the freshly PLD-deposited $LiFePO_4$−C film before annealing treatment. We speculated that the sp^2/sp^3 ratio of carbon was not so homogeneously distributed throughout the as-deposited $LiFePO_4$−C films, which may be responsible for this contradiction. Further work is in progress to clarify this phenomenon.

3.1.4. SEM Analysis. Figure 7a,c shows the surface morphologies of the $LiFePO_4$−C films deposited from target C before and after annealing, respectively. No obvious surface grains structure can be distinguished in the as-deposited film without annealing treatment. After the film was annealed at 600 °C for 6 h, crystals were formed. On the other hand, nonuniform distribution of grain size and cracking leading to the formation of island crystal structures of the film can be observed as shown in Figure 7c. Figure 7b,d shows the cross section of this film, and the thickness of the as-deposited $LiFePO_4$−C films was about 200 nm. The cross-sectional view of the annealed film reveals that part of the film had delaminated from the Si/SiO_2/Ti/Pt substrate after annealing (Figure 7d). The detachment of the film could be a result of a different thermal expansion coefficient between the substrate and the deposited $LiFePO_4$ films as well as the large induced strain due to change of crystal orientation by annealing.

3.1.5. Electrical Conductivity. DC two-probe method was employed to evaluate the electrical conductivity of the samples. The experimental setup was schematically shown in the Supporting Information (Figure S1). To get more reliable results, nine parallel experiments were conducted by varying the gold electrodes, and the mathematical mean was obtained. However, it was hard to get reliable conductivity values for the films after annealing since the result from the annealed films was relatively random and not quite repeatable, which may be due to the highly uneven surface roughness, surface structures, and cracking of the annealed films. The room-temperature electrical conductivities of the $LiFePO_4$−C composite films deposited using targets A, B, and C were calculated to be about 5.2×10^{-10}, 8.8×10^{-9}, and 1.6×10^{-7} $S \cdot cm^{-1}$, respectively. This implies that the electrical conductivity had increased by a factor of $\sim 10^3$ when the mass ratio of PVA was raised from 0.5 wt % to 3 wt % in the target preparation. This is believed to be mainly responsible for the obvious electrochemical activity enhancement of the $LiFePO_4$−C composite cathode films deposited from target C, as will be described in the following section.

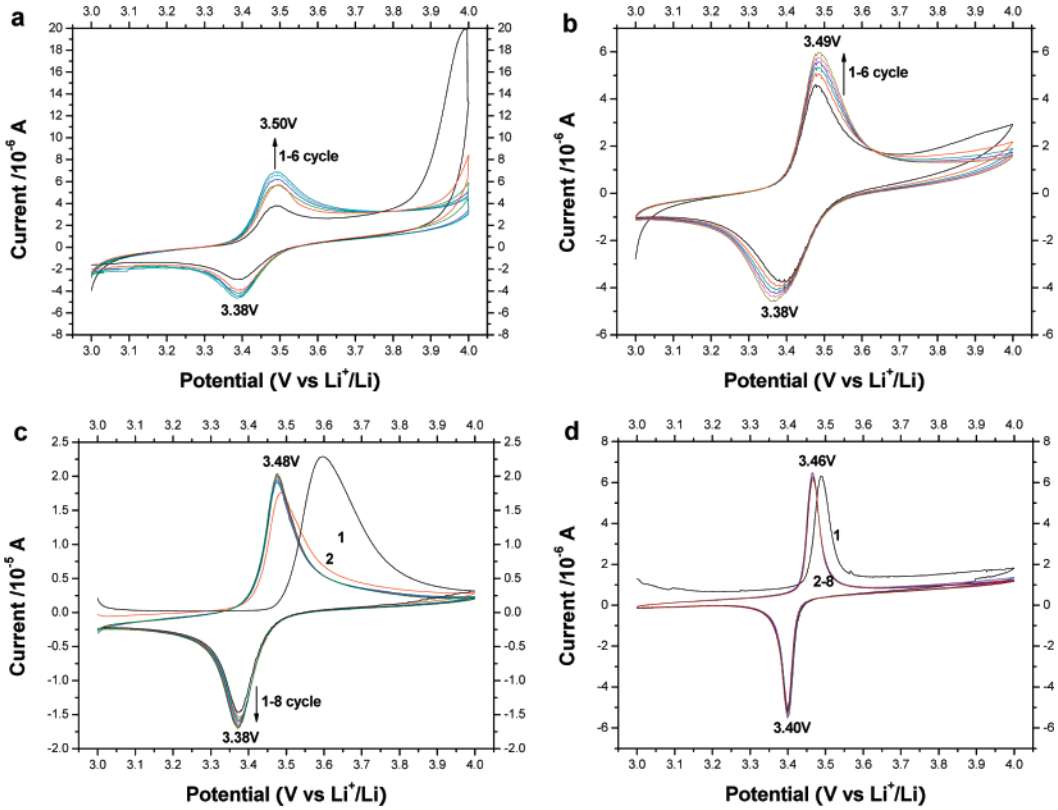

Figure 8. CV cycling test of the $LiFePO_4$−C composite films deposited from (a) target A, (b) target B, and (c) target C, without annealing treatment. (d) CV cycling test of the $LiFePO_4$−C composite films deposited from target C and with annealing treatment. The scan rate was fixed at 0.2 mV/s.

TABLE 1: Summarization of the Raman, XPS, CV, and EIS Results and the Electrochemical Properties as a Function of Carbon Content and Heat Treatment

	PVA content of the target /wt %	G/D ratio from Raman results	G/D ratio from XPS results	rt electrical conductivity /S·cm^{-1}	peak intensity ratio from CV results (cathodic/anodic)/%	ΔE_p/ mV	discharge capacity /μAh·cm^{-2}·μm^{-1}	R_s /Ω	R_{ct} /Ω
target A	0.5			5.2×10^{-10}	67.6	120	<3	10.2	136.7
target B	2			8.8×10^{-9}	77.0	110	~4	8.2	59.6
target C	3	<0.05	0.14	1.6×10^{-7}	83.7	100	~20	6.5	16.2
target C/ annealed	3	0.2	0.82		86.4	60	~10	3.2	10.7

3.2. Electrochemical Characterization. *3.2.1. Cyclic Voltammograms.* The freshly deposited $LiFePO_4$−C composite films were tested by cyclic voltammetry at a scan rate of 0.2 mV/s as depicted in Figure 8. Figure 8a shows the first six CV curves of the film deposited from target A. The peaks observed at 3.50 V in the anodic sweep and 3.38 V in the cathodic sweep are characteristic of the removal and insertion of Li^+ from/into the $LiFePO_4/FePO_4$ structure. However, the initial scanning has additional high residue of anodic current at the higher potential region (from 3.8 to 4.0 V). As the cycling proceeds, this additional current abruptly disappears and the intensity of both anodic and cathodic peaks gradually increases. But this change becomes very small after the fifth cycle. When it became stable, the anodic and cathodic peak intensities were found to be around 6.8 and 4.6 μA, respectively. The potential difference between the anodic and cathodic peaks (ΔE_p) was found to be larger than 120 mV, indicating a serious polarization behavior, which is due to the very limited electrical conductivity of the $LiFePO_4$ films deposited from target A. Figure 8b shows the first six CV cycles of the film deposited from target B. The curves have shape and change inclination similar to that of the film deposited from target A except that the remaining anodic current in the initial cycle was much weaker. After becoming stable, the anodic and cathodic peak intensities were found to be around 6.0 and 4.6 μA, respectively. The ΔE_p value was about 110 mV.

Figure 8c shows eight CV cycles of the film deposited from target C. It reveals that the as-deposited $LiFePO_4$−C composite film has a very high irreversible capacity loss during the initial cycle but attained very good electrochemical reversibility after the third cycle. Song et al.[10] obtained similar CV results, and they attributed the initial high capacity loss to the iron oxide that presents as impurity on the film surfaces, which is verified in the Raman analysis. When they became stable, the anodic and cathodic peak intensities were found to be around 20.3 and 17.0 μA, respectively. The ΔE_p value was reduced to be less than 100 mV. Noticeably, as compared with the films deposited using targets A and B, the film deposited using target C has more intense anodic and cathodic peaks, less polarization (lower ΔE_p), and more symmetric curve (relatively flat baseline), indicating an improved specific capacity and more reversible redox reaction as the increase of conductive carbon content in the as-deposited $LiFePO_4$ films. Figure 8d shows eight CV cycles of the film deposited using target C and with annealing treatment. The initial cycle also has a somewhat residual current in the anodic scanning. But it becomes very stable only after the second cycle. When it became stable, the anodic and

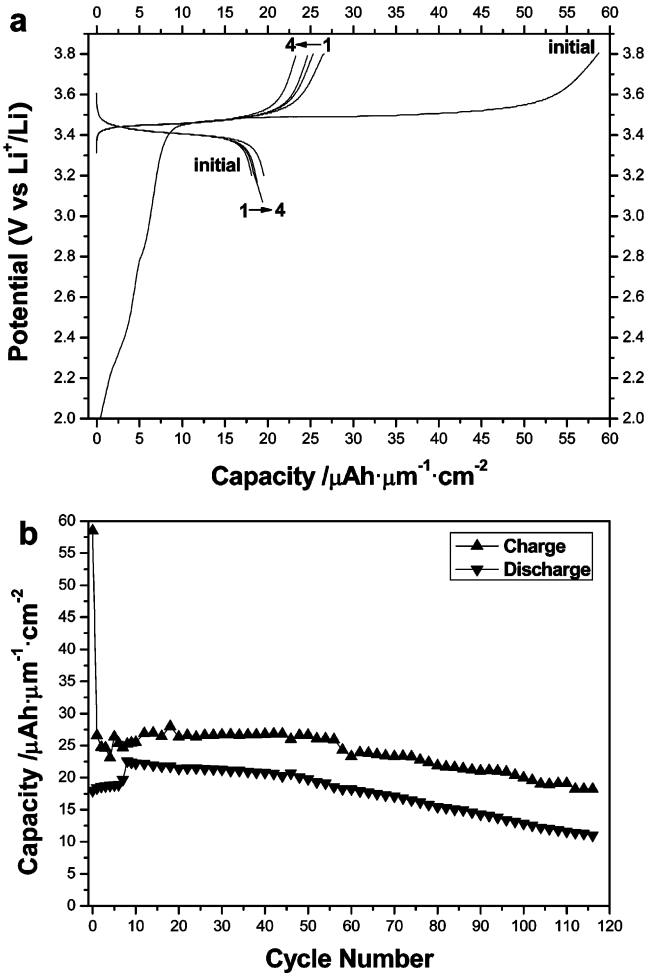

Figure 9. (a) Charge/discharge voltage profile of the $LiFePO_4$−C thin film deposited from target C before annealing. (b) Capacity as a function of cycle number from the initial to the 116th cycle. The charge/discharge current density was fixed at 8 μA/cm^2 (about 0.7 C).

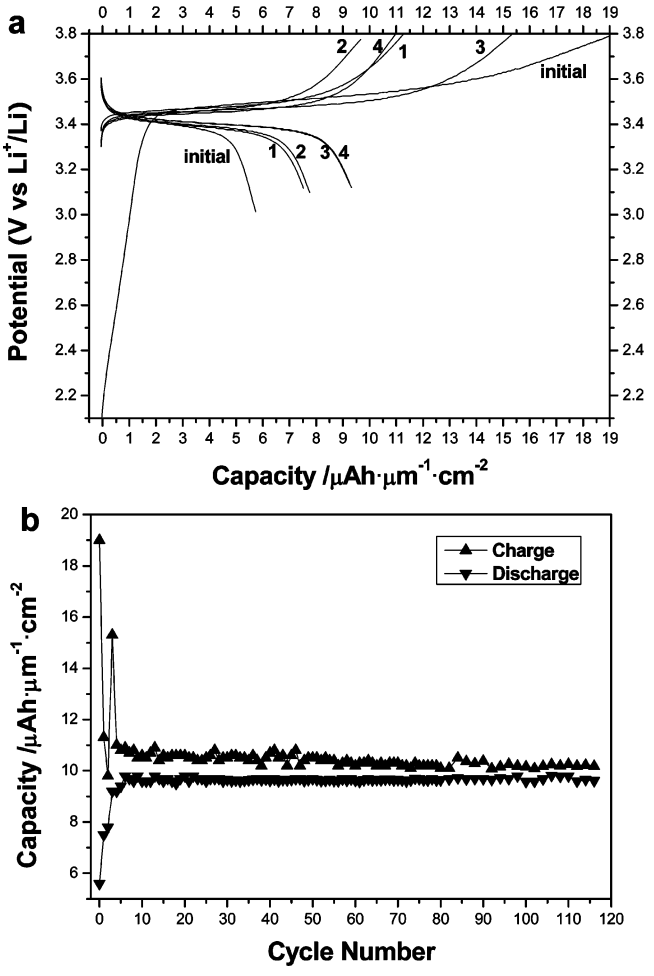

Figure 10. (a) Charge/discharge voltage profile of the $LiFePO_4$−C thin film deposited using target C after annealing at 600 °C for 6 h. (b) Specific capacities as a function of cycle number. The charge/discharge current density was fixed at 8 μA/cm^2 (about 0.7 C).

cathodic peak intensities were found to be about 6.46 and 5.58 μA, respectively. The ΔE_p value was largely decreased to be less than 60 mV. As compared with the films without annealing, both the anodic and cathodic peak intensities were reduced, but the potential difference (ΔE_p) was much narrower, indicating a lower specific capacity but more reversible redox reaction after the annealing treatment. Some characteristic features of the CV analysis were summarized in Table 1. It is obvious that the increase of carbon content in the target had enhanced the electrical conductivity, thus leading to faster electrochemical kinetics of the as-deposited $LiFePO_4$ film electrodes.

3.2.2. Normal Charge and Discharge. It has been found that the expected discharge voltage windows specific to olivine-type $LiFePO_4$ were hard to be detected for the $LiFePO_4$−C composite films deposited using target A (Figure S2). The phenomenon can be correlated to the low electrical conductivity of the as-deposited $LiFePO_4$ films ($\sim 5.2 \times 10^{-10}$ S·cm^{-1}). The $LiFePO_4$−C composite film deposited using target B displays an obvious charge and discharge plateau at around 3.45 and 3.35 V, respectively, corresponding to the typical features of the olivine-type $LiFePO_4$ (Figure S3). However, the Coulombic efficiency (ratio of discharge capacity to charge capacity) at the current density of 8 μA/cm^2 was less than 10%, which was very low. This implies that the electrochemical performances of the $LiFePO_4$−C composite films deposited using target B with a higher fraction of carbon are relatively better than that using target A. Yet, the specific capacities (~ 4 μAh·μm^{-1}·cm^{-2}) are far from enough for practical application. It is proposed that the electrochemical property improvements were mainly contributed by the increase of the carbon fraction, which might have increased the electrical conductivity from 5.2×10^{-10} to $\sim 8.8 \times 10^{-9}$ S·cm^{-1}.

Figure 9a shows the charge/discharge profiles of the $LiFePO_4$−C composite films deposited using target C without postdeposition annealing treatment. Noticeably, the specific discharge capacity was substantially increased to about 20 μAh·μm^{-1}·cm^{-2} and the Coulombic efficiency was greatly improved to be higher than 80% after being activated by the first cycle in addition to the very straightforward and flat electrochemical plateau at around 3.4 V, displaying the typical electrochemical features of the olivine-type $LiFePO_4$. Moreover, as compared with the films deposited using targets A and B, this film shows a very small charge/discharge polarization. The irreversible capacity loss in the initial cycle is consistent with the aforementioned CV analysis and is proposed to be closely associated with the surface impurities[10] that have been described in the Raman section. As discussed in the previous section, the room-temperature electrical conductivity of the films deposited using target C ($\sim 1.6 \times 10^{-7}$ S·cm^{-1}) is higher than that of the films deposited using target A ($\sim 5.2 \times 10^{-10}$ S·cm^{-1}) by a factor of $\sim 10^3$. On the other hand, it has been found that the G/D ratio in the as-deposited $LiFePO_4$−C composite thin films increases with the carbon content in the target, indicating an increase of the amount of larger graphene clusters in the carbon

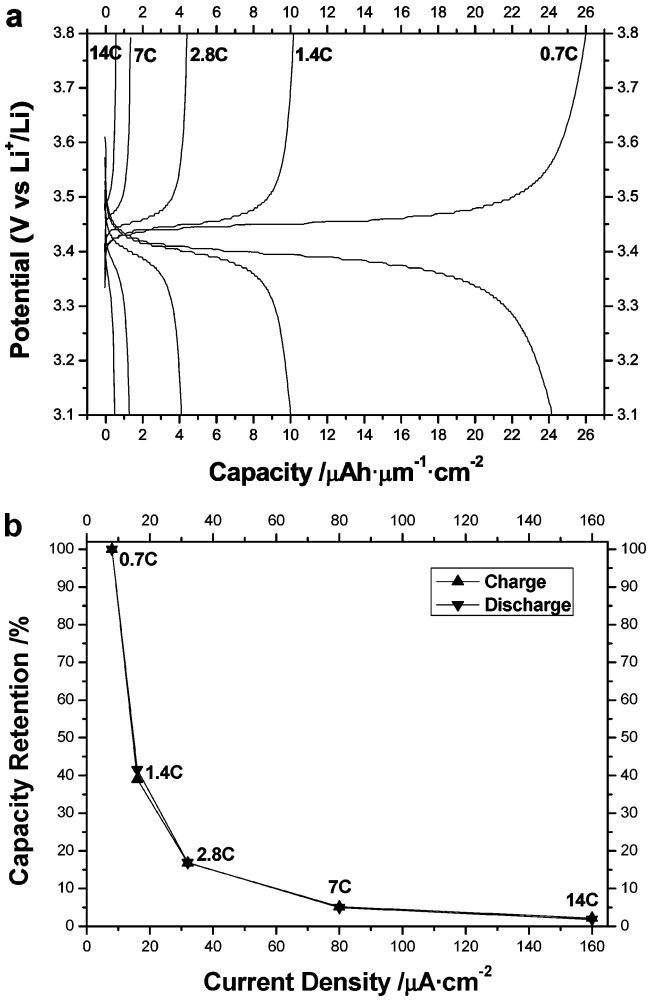

Figure 11. (a) Voltage profiles of the $LiFePO_4$−C films deposited using target C without annealing under various charge/discharge current densities. (b) Capacity remaining ratio of this film under high rate charge/discharge current density as compared to the capacity under 8 $\mu A/cm^2$ (∼0.7 C).

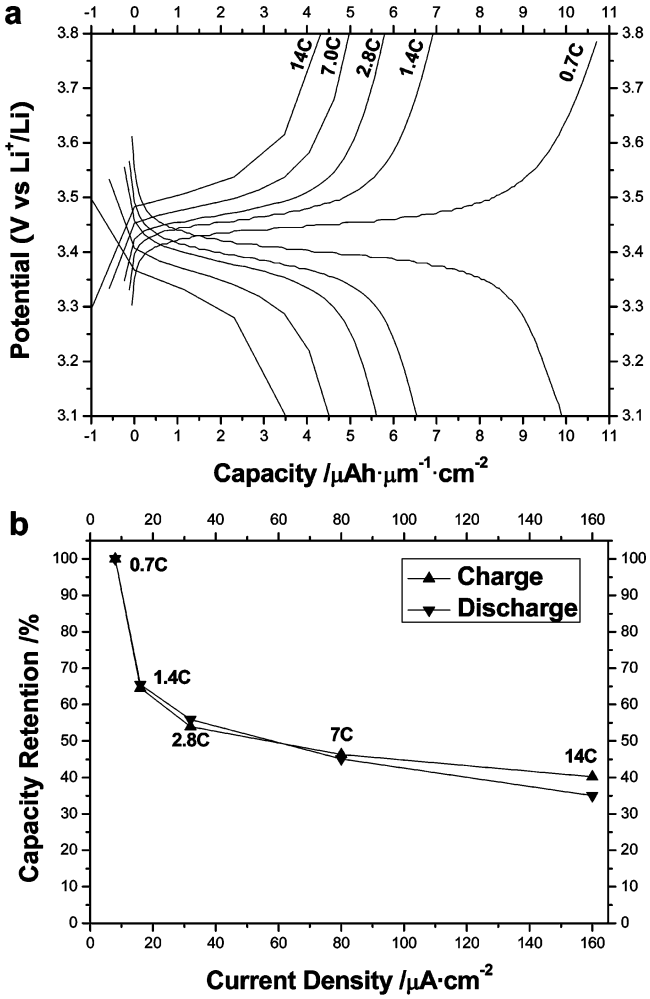

Figure 12. (a) Voltage profiles of the $LiFePO_4$−C films deposited using target C and after annealing at 600 °C for 6 h under various charge/discharge current density. (b) Capacity remaining ratio of this film under high rate charge/discharge current density as compared to the capacity under 8 $\mu A/cm^2$ (∼0.7 C).

structure, and consequently, improved the electronic conductivity of the film cathode.[30,31] These two factors are believed to have contributed substantially to the considerable electrochemical activity enhancement. However, the cycling testing as summarized in Figure 11b indicates that only 45% of the discharge capacity can be retained after 100 cycles, which suggests that the charge/discharge cycling is not so stable relative to the annealed films to be discussed in the following paragraph.

Figure 10a shows the charge/discharge profiles of the $LiFePO_4$−C composite films deposited using target C and after annealing at 600 °C for 6 h. As compared to the film without annealing, the Coulombic efficiency was increased to a high value of more than 95%. Furthermore, no obvious capacity decaying was observed after 115 continuous charge/discharge cycles, indicating an utmost stability of the as-annealed films (Figure 10b). This result can be attributed to the annealing effects, which had increased the ratio in sp^2/sp^3 leading to enhanced electrical conductivity and produced the island-type structure facilitating the intimate contact of the active $LiFePO_4$ films with the electrolyte. However, the capacity was found reduced considerably from 20 to 10.5 $\mu Ah{\cdot}\mu m^{-1}{\cdot}cm^{-2}$ due to the loss of active materials resulting from the detachment of the film from the substrate caused by the different thermal expansion coefficient between the substrate and the $LiFePO_4$ film.

3.2.3. High Rate Charge and Discharge. Figures 11a and 12a illustrate the charge/discharge evolution of the $LiFePO_4$−C composite thin films deposited from target C with and without annealing, respectively, as a function of rate ranging from 0.7 to 14 C. It is clear that, as the current density increases, the specific capacity decreases, while the charge/discharge polarization becomes more pronounced. Under a current density as high as 160 $\mu A/cm^2$ (∼14 C), about 2% and 40% of capacities at low rate (8 $\mu A/cm^2$, ∼0.7 C) can be maintained for the as-deposited $LiFePO_4$−C composite films before and after annealing as summarized in Figures 11b and 12b, respectively. As a result, the high rate (or fast) charge and discharge capability of the as-deposited $LiFePO_4$−C film can be greatly improved after annealing treatment because of the enhancement of electronic conductivity and the formation of island-type film structure.

Different studies have shown that annealing condition plays an important role in determining the electrochemical properties of the $LiFePO_4$ cathode films.[32] The minimum recommended temperature to achieve the olivine phase structure of $LiFePO_4$ was 600 °C. Since the maximum substrate stage heating temperature of the present PLD system is 600 °C, the films were also annealed at higher temperatures of 700, 750, and 800 °C, respectively, for 0.5 h by using a tube furnace under the protective high purity argon atmosphere but without degassing to vacuum before heat treatment. However, it was

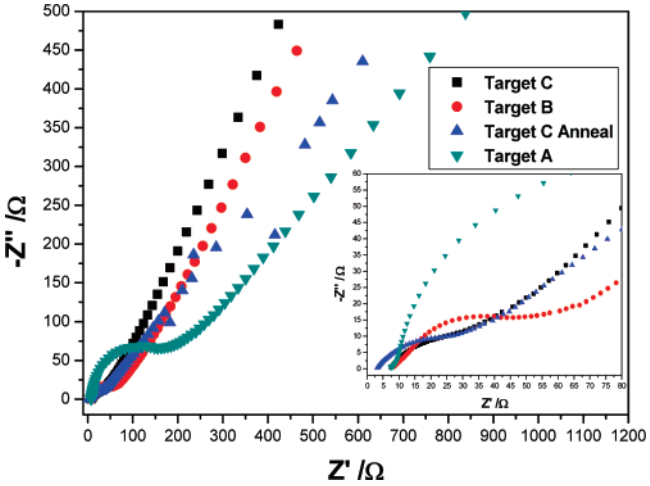

Figure 13. Nyquist plots of the $LiFePO_4$−C composite films deposited using targets A, B, and C, without annealing treatment, and using target C with annealing treatment.

discovered that all the films peeled off from the substrate after annealing in this heat treatment environment. The reason is probably because the expansion coefficient differences between substrate and the $LiFePO_4$ thin films become more severe in the tube furnace environment. Further experiments are required to understand the phenomenon.

3.2.4. Electrochemical Impedance Spectroscopy. EIS was also employed to study the as-deposited $LiFePO_4$−C thin film electrodes. Figure 13 shows the effects of carbon content and annealing treatment on the Nyquist plots of the $LiFePO_4$ films. The inset in Figure 13 is the high-frequency part of the result. The Nyquist plots of all four film samples represent an intercept at high frequency, followed by a depressed semicircle in the high-middle frequency region, and a straight line in the low-frequency range. According to the literature, the intercept impedance on the real resistance axis identifies the Ohmic resistance (R_s) comprising the resistance of the electrolyte and electrode. The depressed semicircle denotes the charge-transfer reaction between the active materials and the electrolyte (R_{ct}). At very low frequencies, they are typical Warburg behavior.[33] The R_s and R_{ct} were calculated by equivalent circuit fitting as shown in the Supporting Information (Figure S4) and summarized in Table 1. It can be seen that both R_s and R_{ct} obviously decrease with the carbon content and postdeposition annealing treatment substantially reduces the R_s and R_{ct} from 6.5Ω and 16.2Ω to 3.2Ω and 10.7Ω, respectively. As the same type electrolyte was used for all the electrode characterization, the R_s and R_{ct} values can be simply used to evaluate the electrical conductivity of the as-deposited thin film electrodes and the Li^+ ion diffusion capability through the solid-electrolyte interface layer. Therefore, raising the conductive carbon content in the original target and in-chamber postdeposition heat treatment can improve the electrical conductivity as well as the Li^+ ion diffusion of the PLD-deposited $LiFePO_4$ films, facilitating faster kinetics of electrochemical reactions, further leading to better electrochemical performances.

4. Conclusions

The work and discussion reported in this article have clearly demonstrated that the increase of conductive carbon content plays a central role in the enhancement of the electrochemical performances of the PLD-deposited $LiFePO_4$ films. Postdeposition annealing treatment was found to improve the Coulombic efficiency as well as the high rate capability considerably. This is probably due to the increase of electrical conductivity and formation of island-type crystalline structures. However, this will also lead to deterioration of the specific capacities, which should be due to the film delamination from the current collectors. To obtain thin film with applicable electrochemical performances, a minimum of 2% carbon content is needed. Although an increase in carbon content was expected to give better electrochemical properties, a too-high carbon content from PVA could lead to problems of shrinkage, thus cracking the target. Additionally, the specific capacities will be lowered if the ratio of carbon/$LiFePO_4$ increases.

Acknowledgment. This work was supported by the CERG grant from the Research Grants Council of the Hong Kong Special Administrative Region, China (CityU 1316/03E). We would like to thank Mr. Zhang Yao from South China University of Technology for his kind help and thoughtful discussion.

Supporting Information Available: Additional experimental details and results. This material is available free of charge via the Internet at http://pubs.acs.org.

References and Notes

(1) (a) Padhi, K.; Nanjundaswamy, K. S.; Goodenough, J. B. *J. Electrochem. Soc.* **1997**, *144*, 1188. (b) Padhi, K.; Nanjundaswamy, K. S.; Masquelier, C.; Okada, S.; Goodenough, J. B. *J. Electrochem. Soc.* **1997**, *144*, 1609.

(2) Tarascon, J. M.; Armand, M. *Nature* **2001**, *414*, 359.

(3) Whittingham, M. S. *Chem. Rev.* **2004**, *104*, 4271.

(4) Ravet, N.; Goodenough, J. B.; Besner, S.; Simoneau, M.; Hovington, P.; Armand, M. Presented at the 206th Meeting of the Electrochemical Society, Honolulu, HI, Oct 1999; p 17.

(5) (a) Ravet, N.; Chouinard, Y.; Magnan, J. F.; Besner, S.; Gauthier, M.; Armand, M. *J. Power Sources* **2001**, *97*−*98*, 503. (b) Chen, Z. H.; Dahn, J. R. *J. Electrochem. Soc.* **2002**, *149*, A1184.

(6) Chung, S. Y.; Bloking, J. T.; Chiang, Y. M. *Nat. Mater.* **2002**, *1*, 123.

(7) Yamada, A.; Chung, S. C.; Hinokuma, K. *J. Electrochem. Soc.* **2001**, *148*, A224.

(8) Delacourt, C.; Poizot, P.; Morcrette, M.; Tarascon, J. M.; Masquelier, C. *Chem. Mater.* **2004**, *16*, 93.

(9) (a) Herle, P. S.; Ellis, B.; Coombs, N.; Nazar, L. F. *Nat. Mater.* **2004**, *3*, 147. (b) Wang, Y. Q.; Wang, J. L.; Nuli, Y. N. *Adv. Funct. Mater.* **2006**, *16*, 2135.

(10) Song, S. W.; Reade, R. P.; Kostecki, R.; Striebel, K. A. *J. Electrochem. Soc.* **2006**, *153*, A12.

(11) Bates, J. B.; Dudney, N. J.; Neudecker, B.; Ueda, A.; Evans, C. D. *Solid State Ionics* **2000**, *135*, 33.

(12) Yu, X. H.; Bates, J. B.; Jellison, G. E.; Hart, F. X. *J. Electrochem. Soc.* **1997**, *144*, 524.

(13) Souquet, J. L.; Duclot, M. *Solid State Ionics* **2002**, *148*, 375.

(14) Ramana, C. V.; Zaghib, K.; Julien, C. M. *Chem. Mater.* **2006**, *18*, 1397.

(15) Yada, C.; Iriyama, Y.; Jeong, S. K.; Abe, T.; Inaba, M.; Qgumi, Z. *J. Power Sources* **2005**, *146*, 559.

(16) Iriyama, Y.; Yokoyama, M.; Yada, C.; Jeong, S. K.; Yamada, I.; Abe, T.; Inaba, M.; Ogumi, Z. *Electrochem. Solid-State Lett.* **2004**, *7*, A340.

(17) Sauvage, F.; Baudrin, E.; Morcrette, M.; Tarascon, J. M. *Electrochem. Solid-State Lett.* **2004**, *7*, A15.

(18) Sauvage, F.; Baudrin, E.; Gengembre, L.; Tarascon, J. M. *Solid State Ionics* **2005**, *176*, 1869.

(19) (a) Sauvage, F.; Baudrin, E.; Laffont, L.; Tarascon, J. M. *Solid State Ionics* **2007**, *178*, 145. (b) Sauvage, F.; Laffont, L.; Tarascon, J. M.; Baudrin, E. *J. Power Sources* **2008**, *175*, 495.

(20) (a) Chiu, K. F. *J. Electrochem. Soc.* **2007**, *154*, A129. (b) Chiu, K. F.; Tang, H. Y.; Lin, B. S. *J. Electrochem. Soc.* **2007**, *154*, A364.

(21) Hong, J.; Wang, C. S.; Dudney, N. J.; Lance, M. J. *J. Electrochem. Soc.* **2007**, *154*, A805.

(22) Ma, J.; Qin, Q. Z. *J. Power Sources* **2005**, *148*, 66.

(23) Lu, Z. G.; Cheng, H.; Lo, M. F.; Chung, C. Y. *Adv. Funct. Mater.* **2007**, *17*, 3885.

(24) Eftekhari, A. *J. Electrochem. Soc.* **2004**, *151*, A1816.

(25) West, W. C.; Whitacre, J. F.; Ratnakumar, B. V. *J. Electrochem. Soc.* **2003**, *150*, A1660.

(26) Yang, S. F.; Zavalij, P. Y.; Whittingham, M. S. *Electrochem. Commun.* **2001**, *3*, 505.
(27) Burba, C. M.; Frech, R. *J. Electrochem. Soc.* **2004**, *151*, A1038.
(28) Paraguassu, W.; Freire, P. T. C.; Lemos, V.; Lala, S. M.; Montoro, L. A.; Rosolen, J. M. *J. Raman Spectrosc.* **2005**, *36*, 213.
(29) Paik, N. *Surf. Coat. Technol.* **2005**, *200*, 2170.
(30) Doeff, M. M.; Hu, Y. Q.; McLarnon, F.; Kostecki, R. *Electrochem. Solid-State Lett.* **2003**, *6*, A207.
(31) Wilcox, J. D.; Doeff, M. M.; Marcinek, M.; Kostecki, R. *J. Electrochem. Soc.* **2007**, *154*, A389.
(32) (a) Huang, X. B. *Acta Phys. Chim. Sin.* **2005**, *21*, 707. (b) Mi, C. H.; Zhao, X. B.; Cao, G. S. *J. Electrochem. Soc.* **2005**, *152*, A483.
(33) Bard, A. J.; Faulkner, L. R. *Electrochemical Methods: Fundamentals and Applications*, 2nd ed.; Wiley & Sons: New York, 2001; pp 228−242.